Rapid Communications

Transverse wobbling in an even-even nucleus

Q. B. Chen [1,*] S. Frauendorf,[2,†] and C. M. Petrache[3,‡]

[1]*Physik-Department, Technische Universität München, D-85747 Garching, Germany*

[2]*Physics Department, University of Notre Dame, Notre Dame, Indiana 46556, USA*

[3]*Centre de Sciences Nucléaires et Sciences de la Matière, CNRS/IN2P3, Université Paris-Saclay, Bât. 104-108, 91405 Orsay, France*

(Received 12 June 2019; revised manuscript received 10 August 2019; published 5 December 2019)

Two new bands built on the two-quasiparticle $\pi(h_{11/2})^2$ configuration of the even-even nucleus ^{130}Ba are investigated using constrained triaxial covariant density functional theory combined with quantum particle rotor model calculations. The energy difference between the two bands, as well as the available electromagnetic transition probabilities $B(M1)_{\rm out}/B(E2)_{\rm in}$ and $B(E2)_{\rm out}/B(E2)_{\rm in}$, are well reproduced. The analysis of the angular momentum geometry reveals that the higher band represents transverse wobbling motion of a two-quasiparticle configuration. This is the first example of two-quasiparticle wobbling bands in an even-even nucleus.

DOI: 10.1103/PhysRevC.100.061301

The wobbling motion, proposed by Bohr and Mottelson [1], is a unique feature of triaxially deformed rotating nuclei. Its analog in classical mechanics is the motion of a free asymmetric top. Uniform rotation about the principal axis with the largest moment of inertia has the lowest energy for a given angular momentum. At slightly larger energy this axis executes harmonic precession oscillations about the space-fixed angular momentum vector. The corresponding quantal energy spectrum is a series of rotational $\Delta I = 2$ bands where the signature of the bands alternates with the increasing number of oscillation quanta n. The $\Delta I = 1$, $n \rightarrow n-1$ $E2$ transitions are collectively enhanced.

The predicted wobbling mode for even-even nuclei has not been experimentally confirmed yet. Instead wobbling bands have been reported in the odd-A mass nuclei where intrinsic angular momentum is involved. Most of them are in odd-proton nuclei: ^{161}Lu [2], ^{163}Lu [3,4], ^{165}Lu [5], ^{167}Lu [6], and ^{167}Ta [7] in the $A \approx 160$ mass region and ^{135}Pr [8,9] in the $A \approx 130$ mass region. Very recently, a wobbling band was also reported in the odd-neutron nucleus ^{105}Pd [10] in the $A \approx 100$ mass region.

So far wobbling mode has only been observed in odd-A nuclei. The energy difference between the wobbling bands has been found to decrease with increasing spin, contrary to the behavior expected for even-even nuclei [1]. Frauendorf and Dönau [11] interpreted this behavior as the consequence of the perpendicular orientation of the odd-particle angular momentum to the axis with the maximal moment of inertia. They called this coupling *transverse* wobbling (TW) to distinguish it from the alternative coupling scheme which corresponds to parallel orientation of the odd particle angular momentum to the axis with the maximal moment of inertia. For this *longitudinal* wobbling mode (LW) the wobbling energy increases with spin.

The evidence for wobbling in even-even nuclei is fragmentary. For instance, Refs. [11,12] for ^{112}Ru and [13] for ^{114}Pd interpreted the "γ bands" as $n = 1$ and 2 wobbling bands, because the energy of their odd-spin members lies below the mean energy of the adjacent even-spin levels. Such a fingerprint is considered as evidence of triaxial deformation [14] (see a detailed discussion in Ref. [15]), for which the wobbling mode develops with increasing spin (cf. [1,11]). However, no electromagnetic transition data were reported to put the wobbling interpretation on solid ground. At present, the appearance of wobbling modes is not yet demonstrated for even-even nuclei.

Very recently, in Ref. [16], a large variety of band structures has been reported in the even-even nucleus ^{130}Ba, out of which a pair of bands with even and odd spins, labeled S1 and S1′, attracted our attention. According to the quasiparticle alignment analysis, the bands are built on two rotational aligned proton $h_{11/2}$ particles. Such a configuration can fulfill the conditions for TW motion.

In this paper, we report a theoretical investigation which suggests that the two newly observed two-quasiparticle bands S1 and S1′ of ^{130}Ba can be interpreted as the zero- and one-phonon states of the TW mode. This is the first example of wobbling motion based on a two-quasiparticle configuration. The analysis of the data shows that the TW regime is much more stable than for the known cases with one odd quasiparticle. That is, we present the best known case for TW.

The experimental information relevant for the present work has been recently reported in Ref. [16], in which the mixing ratios δ of the transitions connecting the two wobbling candidates have been extracted from the analysis of the angular distribution of the γ rays emitted by the excited ^{130}Ba nucleus. The mixing ratios were subsequently used to deduce the

*qbchen@pku.edu.cn

†sfrauend@nd.edu

‡petrache@csnsm.in2p3.fr

TABLE I. Experimental and theoretical mixing ratios δ as well as the transition probability ratios $B(M1)_{\rm out}/B(E2)_{\rm in}$ and $B(E2)_{\rm out}/B(E2)_{\rm in}$ for the transitions from band S1′ to band S1 of ^{130}Ba.

	δ		$\frac{B(M1)_{\rm out}}{B(E2)_{\rm in}}(\frac{\mu_N^2}{e^2b^2})$		$\frac{B(E2)_{\rm out}}{B(E2)_{\rm in}}$	
I ($\hbar$)	Expt	PRM	Expt	PRM	Expt	PRM
13	-0.58^{+13}_{-13}	−0.67	0.36^{+19}_{-13}	1.11	0.32^{+18}_{-15}	0.51
15	-0.62^{+10}_{-10}	−0.68	0.38^{+61}_{-16}	0.90	0.36^{+70}_{-19}	0.42
17	-0.62^{+10}_{-10}	−0.68	0.23^{+22}_{-09}	0.76	0.22^{+27}_{-10}	0.35
19	−0.60	−0.66	0.25^{+23}_{-08}	0.67	0.22^{+21}_{-07}	0.29
21	−0.60	−0.63	0.43^{+35}_{-13}	0.63	0.41^{+34}_{-13}	0.25

$B(M1)_{\rm out}/B(E2)_{\rm in}$ and $B(E2)_{\rm out}/B(E2)_{\rm in}$ ratios of reduced transition probabilities for the $\Delta I = 1$ transitions connecting band S1′ to band S1. The experimental data were obtained from a fusion-evaporation reaction in which ^{130}Ba was populated via the ^{122}Sn(^{13}C, $5n$) reaction at a beam energy of 65 MeV. The mixing ratios δ of the $M1/E2$ transitions were deduced from the transition intensities measured at the four angles available in the GALILEO array [17,18] by employing a method developed by Matta *et al.* [8] for the analysis of angular-distribution measurements. For many transitions there are two solutions for δ in the χ^2 plot, with the absolute values larger than 1 and smaller than 1. For all transitions analyzed in the present work, the δ values smaller than 1 have been adopted, since they have smaller χ^2 values. However, one cannot completely exclude the larger values based only on the angular distribution measurement. On the other hand, such larger values would reinforce the conclusions of the present work. The resulting values are collected in Table I. More experimental details can be found in Refs. [16,19].

To determine the shape, we carried out triaxial constrained covariant density functional theory (CDFT) calculations with the effective interaction PC-PK1 [20]. The details are given in Refs. [21,22]. The configuration $\pi(h_{11/2})^2$ was assigned to bands S1 and S1′, which was fixed by requiring that the overlap between the Slater determinants of adjacent points on the deformation grid had to be larger than 0.9. The minimum was found at the triaxial shape with ($\beta = 0.24, \gamma = 21.5°$) and an excitation energy of 3.13 MeV with respect to the ground state ($\beta = 0.23, \gamma = 14°$), which favorably compares with the experimental excitation energy of 3.79 MeV of the $I = 10$ state of band S1. To check the angular momentum dependence of the shape, we carried out tilted axis cranking (TAC) calculations [23] assuming zero proton pairing and varying neutron paring. The deformation changes are minor and not very sensitive to the neutron pairing. For $I = 14 \rightarrow 24$ we found that $(\beta, \gamma) = (0.23, 30°) \rightarrow (0.20, 26°)$ for $\Delta_n = 0$ and $(0.21, 24°) \rightarrow (0.20, 29°)$ for $\Delta_n = 0.8$ MeV. At fixed deformation, the dynamic moment of inertia $\mathcal{J}^{(2)} = dI/d\omega$ is about constant for $\Delta_n = 0$ and increases for $\Delta_n > 0$, where the rate sensitively depends on Δ_n.

We performed particle rotor model (PRM) [11,24–26] calculations for the adopted $\pi(h_{11/2})^2$ configuration and the

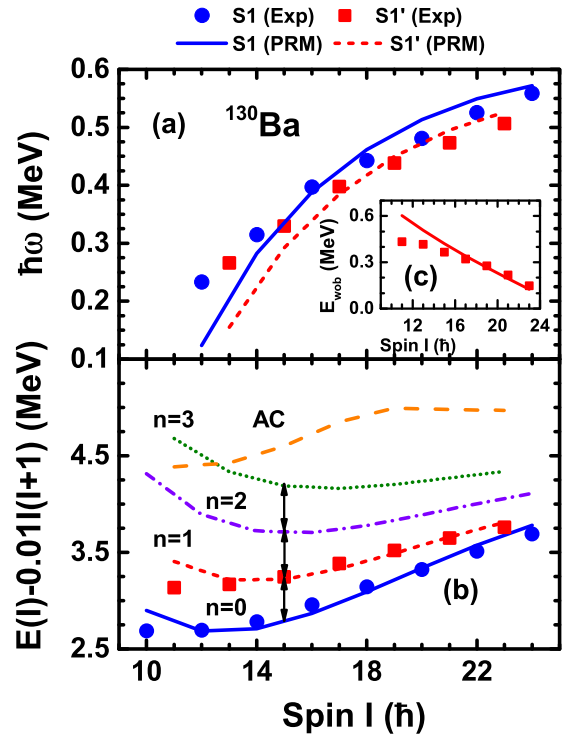

FIG. 1. Energetics of the lowest bands based on the $\pi(h_{11/2})^2$ in ^{130}Ba. (a) Experimental and PRM rotational frequency for the bands S1 and S1′. (b) PRM energies minus a common rigid rotor reference. The bands based on the lowest $\pi(h_{11/2})^2$ configuration AB are labeled by the wobbling phonon number n assigned to them. The $n = 0$ band based on the excited $\pi(h_{11/2})^2$ configuration is labeled by AC. The known experimental energies are included. (c) Wobbling energies $E_{\rm wob}(I) = E_{n=1}(I) - [E_{n=0}(I+1) + E_{n=0}(I-1)]/2$ obtained by PRM compared with the experimental values obtained from bands S1 ($n = 0$) and S1′ ($n = 1$).

CDFT deformation parameters ($\beta = 0.24, \gamma = 21.5°$). The protons are described by a single-j shell Hamiltonian [27] assuming zero pairing. The triaxial rotor is parametrized by the three spin-dependent moments of inertia $\mathcal{J}_i = \Theta_i(1 + cI)$, in which $i = s$, m, l denotes the short, medium, and long axes, respectively. The parameters Θ_s, Θ_m, Θ_l = 1.09, 1.50, 0.65 $\hbar^2$/MeV and $c = 0.59$ are determined by adjusting the PRM energies to the experimental energies of the zero- and one-phonon bands. The spin dependence is attributed to the presence of neutron pairing. The fitted ratios $\mathcal{J}_s/\mathcal{J}_m/\mathcal{J}_l = 0.73/1.00/0.43$, different from the ratios 0.40/1.00/0.14 for the irrotational flow type moments of inertia [27]. The larger ratio $\mathcal{J}_s/\mathcal{J}_m$ stabilizes the TW mode. Microscopic cranking calculations give the larger ratio $\mathcal{J}_s/\mathcal{J}_m = 0.60/1.00$ [28]. One also has to take into account that the deformation represents an average value, around which substantial fluctuations exist. These reduce $\mathcal{J}_m$ from its irrotational flow value for the average γ value (see Fig. 1 of [28]). Modifying the deformation parameters within the range found by the TAC calculations and keeping $\mathcal{J}_i$ the same did not change the results in a substantial way. For the electromagnetic transitions we used the intrinsic quadrupole moments $Q_0 = Q\cos\gamma$ and $Q_2 = Q\sin\gamma/\sqrt{2}$

with $Q = (3/\sqrt{5\pi})R_0^2 Z\beta$, $R_0 = 1.2A^{1/3}$ fm, and the gyromagnetic ratios $g_R = Z/A = 0.43$ for the rotor and $g_\pi(h_{11/2}) = 1.21$ for the protons.

The calculated rotational frequency $\hbar\omega(I) = [E(I) - E(I-2)]/2$ and energy $E(I)$ spectra for bands S1 and S1′, in comparison with the experimental data, are shown in Fig. 1. It is seen that the PRM calculations reproduce well the bands S1 and S1′. In agreement with the experimental observation, the calculated wobbling energy $E_{\rm wob}(I)$ decreases in the whole spin region, providing evidence for TW motion.

The experimental and theoretical mixing ratios δ as well as the transition probability ratios $B(M1)_{\rm out}/B(E2)_{\rm in}$ and $B(E2)_{\rm out}/B(E2)_{\rm in}$ for the transitions from band S1′ to S1 are compared in Table I. The calculated $B(E2)_{\rm out}/B(E2)_{\rm in}$ values agree with experiment within the uncertainties. The $B(E2)_{\rm out}/B(E2)_{\rm in}$ is proportional to $\tan^2\gamma$ [1]. The PRM calculations using $\gamma = 21.5^\circ$ can reproduce the experimental $B(E2)_{\rm out}/B(E2)_{\rm in}$ value. Thus, the microscopic input of the triaxial deformation parameter from the CDFT calculation is appropriate. The large ratios indicate that the $E2$ transitions from S1′ to S1 are highly collective. This is the fingerprint of TW, which represents a wobbling of the triaxial charge density with respect to the angular momentum vector. The theoretical $B(M1)_{\rm out}/B(E2)_{\rm in}$ ratios are somewhat on the large side compared to experiment.

Note that in comparison with TW in odd-A nuclei, as ^{135}Pr [8,9] and ^{105}Pd [10], the $B(M1)_{\rm out}/B(E2)_{\rm in}$ in ^{130}Ba is about three times larger. This is attributed to the fact that one more high-j quasiparticle is involved in the configuration of the S1 and S1′ bands, which enlarges the $M1$ matrix elements. As a consequence, the relative contribution of the $E2$ component to the $\Delta I = 1$ transitions [calculated as $\delta^2/(1+\delta^2)$] is smaller ($\approx$25%) and does not dominate like in the case of the one-quasiparticle bands of the odd-even wobbling nuclei.

The overestimation of the $B(M1)_{\rm out}$ has already been observed in the PRM calculations for ^{135}Pr [8,11] and the Lu isotopes [11]. According to the quasiparticle-random-phase approximation (QRPA) calculations [29], the wobbling motion is not a pure orientation vibration of the quadrupole mass tensor with respect to the angular momentum vector, but also coupled to the vibrations of the proton and neutron currents against each other, i.e., the scissor mode. The coupling to the scissor draws $M1$ strength from the TW mode, which is not taken into in the PRM.

Figure 2 shows the probability density distributions $\mathcal{P}(\theta,\varphi)$ for the orientation of the angular momenta $\boldsymbol{J}$ with respect to the body-fixed frame [26,30–32] at spins $I = 14$ and 15, respectively. Figure 3 shows the rms components along the medium, short, and long axes of the $\boldsymbol{R}$, of the valence protons $\boldsymbol{J}_\pi$, and of the total angular momentum $\boldsymbol{I}$, for the bands S1 and S1′.

The figures corroborate the scenario of stable TW. The distributions $\mathcal{P}(\theta,\varphi)$ are centered with the $\theta = 90^\circ$ plane, corresponding to the very small l component of $\boldsymbol{I}$ in Fig. 3. The $n = 0$ state has a maximum at $\varphi = 0^\circ$ corresponding to the maximal alignment of $\boldsymbol{I}$ with the s axis allowed by quantum mechanics. The $n = 1$ state has a minimum there. The maximal probabilities lie on a rim revolving the minimum, which reflects the wobbling motion (precession) of $\boldsymbol{I}$

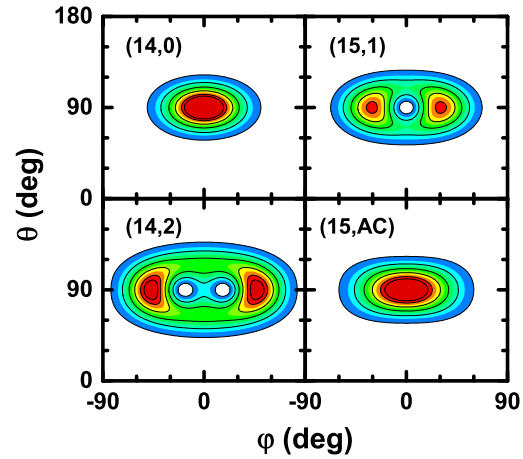

FIG. 2. Distributions of the probability $\mathcal{P}(\theta,\varphi)$ for the orientation of the angular momentum $\boldsymbol{J}$ with respect to the body-fixed frame ("azimuthal plots"). Brown indicates maximal and white minimal probability. Contour lines show equal differences of the probability density. Here, θ is the angle between $\boldsymbol{J}$ and the l axis, and φ is the angle between the projection of $\boldsymbol{J}$ onto the sm plane and the s axis. Due to the D_2 symmetry, $\mathcal{P}(\theta,\varphi)$ is an even function of φ with a period of π. In accordance with Fig. 1, the panels are labeled by (I,n).

about the s axis. These are the expected distributions for the φ-symmetric $n = 0$ and φ-antisymmetric $n = 1$ states. The fact that the distributions centered at $\varphi = 0^\circ$ and $\varphi = \pm 180^\circ$ do not merge at $\varphi = \pm 90^\circ$ indicates that the TW mode is stable.

Figure 3 illustrates how the rms components of $\boldsymbol{R}$, $\boldsymbol{J}_\pi$, and $\boldsymbol{I}$ change with I. The $\boldsymbol{J}_\pi$ of valence proton particles tends to align with the s axis, which corresponds to maximal overlap with the triaxial core [33]. The s component is constant $9.5\hbar$ and $9\hbar$ for S1 and S1′, respectively. The transverse geometry is more stable than for the one-proton bands, where a tilt of the proton angular momentum toward the m axis appears [26,32].

The l component of $\boldsymbol{R}$ stays small because the moment of inertia for rotation around the l axis is the smallest. In order to lower the energy, $\boldsymbol{R}$ favors the sm plane. For band S1, it increases more along the s axis than along the m axis. Combined with $\boldsymbol{J}_\pi$, the s component of $\boldsymbol{I}$ is larger than

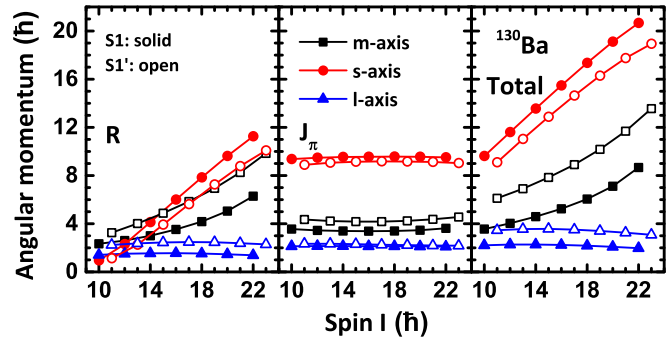

FIG. 3. Root mean square angular momentum components along the medium, short, and long axes of the rotor $\boldsymbol{R}$, valence protons $\boldsymbol{J}_\pi$, and total angular momentum $\boldsymbol{I}$ for the bands S1 and S1′.

the m component. For band S1′, the s and m components of the rotor are about the same. This is attributed to the fact that the transverse wobbling excitation is achieved by adding a rotor angular momentum component along the m axis [26]. The instability point of TW, above which $\boldsymbol{I}$ increases by adding $\boldsymbol{R}$ along the m axis, is not reached, which is consistent with the continued downward trend of the wobbling frequency seen in Fig. 1.

As suggested by the labeling in Fig. 1, the next higher bands are interpreted as the $n = 2$ and $n = 3$ wobbling excitations. In particular for $12 \leqslant I \leqslant 18$, the approximately equal energy spacing provokes the multiphonon interpretation. In accordance with this interpretation, Fig. 2 shows for the $n = 2$ band a rim of $\mathcal{P}(\theta = 90^\circ, \varphi)$ revolving $\varphi = 0$. Its distance to the origin is larger, which reflects the wider precession cone of the $n = 2$ wobbling excitation. The maximum at $\varphi = 0$ between two symmetrically located minima is the topology of a φ-symmetric wave function with two nodes. The distribution $\mathcal{P}(\theta, \varphi)$ for the $n = 3$ band (not shown) has a yet wider rim and a minimum at $\varphi = 0^\circ$ between two symmetrically located maxima and two symmetrically located minima farther out, which is the topology of a $n = 3$ wave function with three nodes.

The calculated $B(E2)_{\rm out}$ and $B(M1)_{\rm out}$ values for the $n = 1$, 2, and 3 bands are shown in Fig. 4. As expected, the $B(E2, n \to n-1)_{\rm out}$ and $B(M1, n \to n-1)_{\rm out}$ values increase with the phonon number n, though more slowly than the harmonic limit $\propto n$. For a simple triaxial rotor the harmonic limit is approached with increasing angular momentum, because the amplitude of the wobbling motion $\propto 1/\sqrt{I}$ [1]. For the TW mode this trend is counteracted by the approach of the critical angular momentum for instability. The transitions $n \to n-2$, which are forbidden in the harmonic limit, are strongly reduced compared with the allowed ones.

Adopting cranked-shell-model terminology, we call the lowest three $h_{11/2}$ proton orbitals in the rotating potential A, B, and C, which have the respective signatures $\alpha = -1/2$, $1/2$, $-1/2$. Then S1 is the $\alpha = 0$ configuration [AB]. The two protons may combine to the $\alpha = 1$ odd-I configuration [AC]. Figure 2 shows that $\boldsymbol{I}$ is aligned with the short axis, similar to [AB]. As seen in Fig. 1, the AC band lies about 2 MeV above the AB band S1. Figure 4 shows that the $B(E2)_{\rm out}$ and $B(M1)_{\rm out}$ values that connect the AC band with S1 are much smaller than the ones that connect the $n = 1$ wobbling excitation S1′ with S1. This is analogous to the case of ^{135}Pr, where strong $B(E2)_{\rm out}$ and $B(M1)_{\rm out}$ values connect the $n = 1$ wobbling band with the yrast band whereas the signature partner band has very weak connecting transitions that are not seen in experiment [8].

In summary, the pair of newly observed bands S1 and S1′ built on the $\pi(h_{11/2})^2$ configuration in ^{130}Ba were investigated

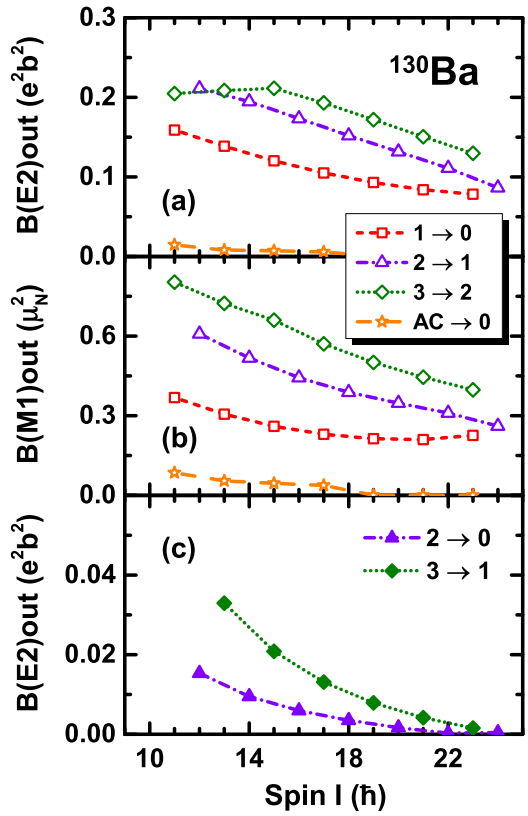

FIG. 4. Calculated $B(E2)$ and $B(M1)$ values for interband transitions: (a) $B(E2)_{\rm out}(n, I \to n-1, I-1)$, (b) $B(M1)(n, I \to n-1, I-1)$, and (c) $B(E2)_{\rm out}(n, I \to n-2, I-2)$.

combining triaxial CDFT with quantum PRM calculations. The experimental energy spectra, energy difference between the two bands, as well as the available electromagnetic transition probabilities $B(M1)_{\rm out}/B(E2)_{\rm in}$ and $B(E2)_{\rm out}/B(E2)_{\rm in}$ are well reproduced. The collective enhancement of the interband $E2$ transitions is clear evidence of the wobbling character of the higher band. The detailed analysis of the angular momentum geometry demonstrates the stable TW character of the excited bands, which makes it the first example for TW based on a two-quasiparticle configuration in an even-even nucleus and the most stable TW case observed so far.

This work was supported by Deutsche Forschungsgemeinschaft (DFG) and National Natural Science Foundation of China (NSFC) through funds provided to the Sino-German CRC 110 "Symmetries and the Emergence of Structure in QCD" (DFG Grant No. TRR110 and NSFC Grant No. 11621131001), and U.S. DOE Grant No. DE-FG02-95ER4093.

[1] A. Bohr and B. R. Mottelson, *Nuclear Structure* (Benjamin, New York, 1975), Vol. II.

[2] P. Bringel, G. B. Hagemann, H. Hübel, A. Al-khatib, P. Bednarczyk, A. Bürger, D. Curien, G. Gangopadhyay, B. Herskind, D. R. Jensen *et al.*, Eur. Phys. J. A **24**, 167 (2005).

[3] S. W. Ødegård, G. B. Hagemann, D. R. Jensen, M. Bergström, B. Herskind, G. Sletten, S. Törmänen, J. N. Wilson, P. O. Tjøm, I. Hamamoto *et al.*, Phys. Rev. Lett. **86**, 5866 (2001).

[4] D. R. Jensen, G. B. Hagemann, I. Hamamoto, S. W. Ødegård, B. Herskind, G. Sletten, J. N. Wilson, K. Spohr, H. Hübel, P. Bringel *et al.*, Phys. Rev. Lett. **89**, 142503 (2002).

[5] G. Schönwaßer, H. Hübel, G. B. Hagemann, P. Bednarczyk, G. Benzoni, A. Bracco, P. Bringel, R. Chapman, D. Curien, J. Domscheit *et al.*, Phys. Lett. B **552**, 9 (2003).
[6] H. Amro, W. C. Ma, G. B. Hagemann, R. M. Diamond, J. Domscheit, P. Fallon, A. Gorgen, B. Herskind, H. Hübel, D. R. Jensen *et al.*, Phys. Lett. B **553**, 197 (2003).
[7] D. J. Hartley, R. V. F. Janssens, L. L. Riedinger, M. A. Riley, A. Aguilar, M. P. Carpenter, C. J. Chiara, P. Chowdhury, I. G. Darby, U. Garg *et al.*, Phys. Rev. C **80**, 041304(R) (2009).
[8] J. T. Matta, U. Garg, W. Li, S. Frauendorf, A. D. Ayangeakaa, D. Patel, K. W. Schlax, R. Palit, S. Saha, J. Sethi *et al.*, Phys. Rev. Lett. **114**, 082501 (2015).
[9] N. Sensharma, U. Garg, S. Zhu, A. D. Ayangeakaa, S. Frauendorf, W. Li, G. Bhat, J. A. Sheikh, M. P. Carpenter, Q. B. Chen *et al.*, Phys. Lett. B **792**, 170 (2019).
[10] J. Timár, Q. B. Chen, B. Kruzsicz, D. Sohler, I. Kuti, S. Q. Zhang, J. Meng, P. Joshi, R. Wadsworth, K. Starosta *et al.*, Phys. Rev. Lett. **122**, 062501 (2019).
[11] S. Frauendorf and F. Dönau, Phys. Rev. C **89**, 014322 (2014).
[12] J. H. Hamilton, S. J. Zhu, Y. X. Luo, A. V. Ramayya, S. Frauendorf, J. O. Rasmussen, J. K. Hwang, S. H. Liu, G. M. Ter-Akopian, A. V. Daniel *et al.*, Nucl. Phys. A **834**, 28c (2010).
[13] Y. X. Luo, J. H. Hamilton, A. V. Ramayya, J. K. Hwang, S. H. Liu, J. O. Rasmussen, S. Frauendorf, G. M. Ter-Akopian, A. V. Daniel, and Y. T. Oganessian, in *Exotic Nuclei: Exon-2012: Proceedings of the International Symposium* (World Scientific, Singapore, 2013).
[14] N. V. Zamfir and R. F. Casten, Phys. Lett. B **260**, 265 (1991).
[15] S. Frauendorf, Int. J. Mod. Phys. E **24**, 1541001 (2015).
[16] C. M. Petrache, P. M. Walker, S. Guo, Q. B. Chen, S. Frauendorf, Y. X. Liu, R. A. Wyss, D. Mengoni, Y. H. Qiang, A. Astier *et al.*, Phys. Lett. B **795**, 241 (2019).
[17] J. J. Valiente-Dobon *et al.*, INFN LNL Annual Report, 2014 (unpublished).
[18] D. Testov *et al.*, in *Exotic nuclei: Exon-2018: Proceedings of the International Symposium* (World Scientific, Singapore, 2019).
[19] Y. H. Qiang, C. M. Petrache, S. Guo, P. M. Walker, D. Mengoni, Q. B. Chen, B. F. Lv, A. Astier, E. Dupont, M. L. Liu *et al.*, Phys. Rev. C **99**, 014307 (2019).
[20] P. W. Zhao, Z. P. Li, J. M. Yao, and J. Meng, Phys. Rev. C **82**, 054319 (2010).
[21] J. Meng, J. Peng, S. Q. Zhang, and S.-G. Zhou, Phys. Rev. C **73**, 037303 (2006).
[22] J. Meng (Ed.), *Relativistic density functional for nuclear structure*, *Vol. 10 of International Review of Nuclear Physics* (World Scientific, Singapore, 2016).
[23] S. Frauendorf, Nucl. Phys. A **677**, 115 (2000).
[24] I. Hamamoto, Phys. Rev. C **65**, 044305 (2002).
[25] W. X. Shi and Q. B. Chen, Chin. Phys. C **39**, 054105 (2015).
[26] E. Streck, Q. B. Chen, N. Kaiser, and U.-G. Meißner, Phys. Rev. C **98**, 044314 (2018).
[27] P. Ring and P. Schuck, *The Nuclear Many Body Problem* (Springer-Verlag, Berlin, 1980).
[28] S. Frauendorf, Phys. Rev. C **97**, 069801 (2018).
[29] S. Frauendorf and F. Dönau, Phys. Rev. C **92**, 064306 (2015).
[30] F. Q. Chen, Q. B. Chen, Y. A. Luo, J. Meng, and S. Q. Zhang, Phys. Rev. C **96**, 051303(R) (2017).
[31] Q. B. Chen and J. Meng, Phys. Rev. C **98**, 031303(R) (2018).
[32] Q. B. Chen and S. Frauendorf (unpublished).
[33] S. Frauendorf and J. Meng, Z. Phys. A **356**, 263 (1996).